Analysis of an integrated tunable spectrometer for the short to mid-infrared range based on a ring resonator

Jie Huang (黄 杰)[1], Junbo Yang (杨俊波)[1,2,*], Hailiang Zhang (张海良)[1], Hongqing Wang (王宏庆)[1], Wenjun Wu (吴闻军)[1], DingBo Chen (陈丁博)[1], and Shengli Chang (常胜利)[1]

[1]*Center of Material Science, National University of Defense Technology, Changsha 410073, China*
[2]*State Key Laboratory on Advanced Optical Communication Systems and Networks, Peking University, Beijing 100871, China*
**Corresponding author: yangjunbo008@sohu.com*

Received June 15, 2016; accepted August 5, 2016; posted online September 2, 2016

An integrated, tunable spectrometer based on a silicon-on-sapphire platform is designed at wavelengths of 2.29–2.35 μm. Its pivotal component is a 4.7 μm-radius ring resonator on a graphene monolayer. Its full width at half-maximum and free spectral range are ∼1.5 and ∼45 nm, respectively, as found through a numerical simulation and theoretical computation. Sixteen characteristic peaks are obtained by tuning the Fermi level of graphene. The gap between the ring and waveguides is increased by 0.5 μm to increase the resolution, and though this can drastically reduce the transmission rate, an upper sapphire layer maintains light to the drop port.

OCIS codes: 130.7408, 130.3120, 130.3990, 140.4780.
doi: 10.3788/COL201614.101301.

The development of micro-nano technology, and in particular high-energy light sources and high-precision detectors, has seen the application of micro-nano devices gradually expand from the near-infrared (NIR) into mid-infrared (MIR) wavelengths. As a result, the high sensitivity and low power consumption of micro-nano photonic sensors[1,2] have received increasing attention from scientific workers. The integrated on-chip spectrometer has been the focus of many researchers as a typical type of passive micro-nano device, and in recent years, structures such as arrayed-waveguide gratings[3–8], planar concave gratings[5,9,10], Mach–Zehnder interferometers[11,12], and micro-ring resonator arrays[13] have been proposed. The resolution of these structures can be very high and often works in the range of tens of nanometers. For example, the linewidth of a previously proposed spectrometer[13] is about 0.6 nm, with an operating bandwidth that can reach 50 nm. Unfortunately, there are still some problems with such structures in terms of producing arrayed-waveguide gratings and ring resonator arrays; i.e., any given channel of the spectrometer can only output one specific spectrum signal. Thus, for a spectrometer to have dozens of characteristic peaks requires a very complicated production process that could limit their practical application. Besides, the response speed of the thermo-optic effect can only reach the microsecond level[14,15], which could be harmful for the improvement of the data transmission speed of a light network.

As a new type of two-dimensional material, graphene has been receiving increasing intention since it was first prepared in 2004. The reason for this is that not only can its conductivity be fleetly and dynamically tuned by electrostatics[16,17], but it can also interact with visible and infrared wavelengths of light[18]. To reduce the difficulty in fabricating on-chip spectrophotometers, this Letter proposes a device based on only one micro-ring resonator. In order to make this work, it is necessary to tune the resonance wavelength of the resonator. This has been achieved by tuning the Fermi level of graphene (i.e., modulating its electro-optic characteristics) in such a way that the resonator can resonate at a specified position[16]. Through structure optimization, we obtained a micro-ring resonator with superior performance and with a working wavelength of 2.29 to 2.35 μm. The three-dimensional finite-difference time-domain (3D FDTD) method was then used to calculate the optical field distribution after light passed through the spectrometer without graphene. Using these results, and the transfer matrix method[19] with the fully vectorial calculation (FVC) method, we analyzed the relationship between the position of resonance peaks and the Fermi level of graphene. The results obtained revealed that it is possible to dynamically modulate the resonance wavelength of a resonator by changing the Fermi level of graphene. This makes it possible to get 16 evenly spaced characteristic peaks within the working wavelength.

A schematic diagram of the pivotal component in the newly proposed micro-ring resonator is provided in Fig. 1, where $h_3 = 4$ μm and $h_2 = 2$ μm are the thicknesses of the silicon and sapphire, respectively. The radius of the resonator is $R = \frac{1}{2}(r_2 + r_1) = 4.7$ μm, which gives a total width of 580 nm. This size was chosen to ensure that the spectrometer can work in the mid-infrared range. The height of the resonator and straight waveguides are 440 nm, the length and width of the two waveguides are 24 μm and 580 nm, and the gaps between the resonator

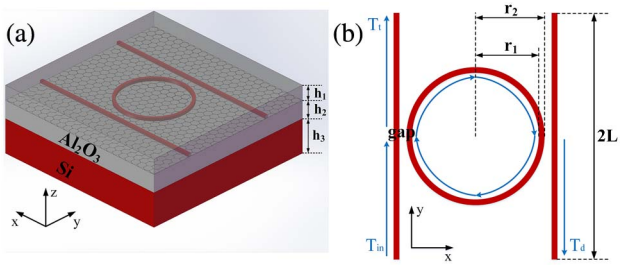

Fig. 1. Schematic diagram of the spectrometer.

and two waveguides are 500 nm. In order to regulate the location of the resonance peaks, a graphene monolayer ~0.5 nm thick was applied onto the sapphire. Finally, an additional layer of sapphire with a thickness of $h_1 = 2$ μm was applied on the top of the graphene in order to strengthen the constraint of light.

The 3D FDTD method was used to calculate the transmission of the drop port (T_d) without graphene. For this, the incident light is assumed to be transverse magnetic (TM) polarized with a wavelength of 2.29 to 2.35 μm. The FVC method was used to calculate the electric field distribution of the cross section and the effective refractive indexes of different wavelengths. According to previous studies[20], the resonance equation of a ring resonator can be expressed as

$$2\pi R n_c = m\lambda, \tag{1}$$

where R is the radius of the resonator, n_c is the effective refractive index, which is dependent on the wavelength of incident light, m is a positive integer related to the resonance order, and λ is the resonant wavelength. Based on the result of the FVC method, the following expression[19] (transfer matrix method) can then be used to fit the transmission of the drop port:

$$T = \left[\frac{-k^2 \exp[-i(\beta - i\alpha)\pi R]}{1 - t^2 \exp[-2i(\beta - i\alpha)\pi R]} \exp[-2i(\beta - i\alpha)L]\right]^2, \tag{2}$$

where k^2 is the power coupling coefficient, t^2 is the power transmission coefficient, and $k^2 + t^2 = 1$ if no coupling loss exists in the coupling region. $\beta = 2\pi n_c/\lambda$ is the propagation constant for both the ring resonator and waveguides, $2L = 24$ μm is the length of the input and output channels, and α is the loss per unit length.

The blue line in Fig. 2(a) shows the transmission curve of the drop port, from which we can see that there are two resonance peaks with a full width at half-maximum (FWHM) of about 1.5 nm. According to the result of FVC method, we can calculate the free spectral range (FSR), which is about 45 nm in the operation's wavelength range. Figure 2(a) also shows that the results of the transfer matrix method and FDTD method are a little different. The locations of the resonance peaks of the transfer matrix method are blue shifted, which is because the dispersion relation used in FDTD is a little different from FVC. The intensity of the second resonance peak is slightly

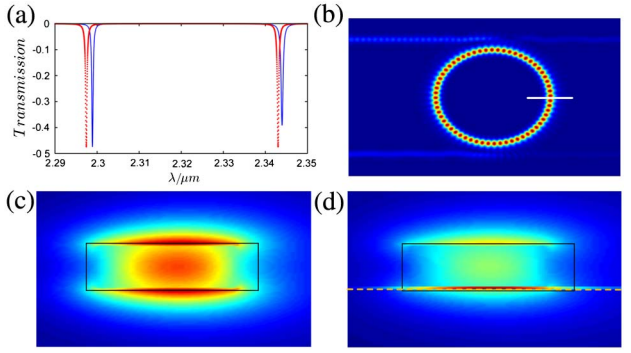

Fig. 2. (a) Transmission curve of the drop port obtained using the FDTD method (blue solid line) and transfer matrix method (red dotted line). (b) Electric field distribution of the resonator at the resonant position ($\lambda = 2.2989$ μm). (c, d) Electric field distribution of the cross section (white line in (b)) without and with single-layer graphene, respectively. The black rectangles in (c) and (d) represent the position of waveguide, and the orange dashed line in (d) represents the position of the single-layer graphene.

different, which is because the wavelength has a strong influence on the loss when using the FDTD method, and we set this value to be constant in the transfer matrix method ($\alpha = 2.71 \times 10^{-4}$ μm^{-1}). Figures 2(c)–2(d) illustrate that the graphene layer has a strong effect on the fundamental TM mode of the waveguide. In addition, Fig. 2(b) shows that the resonant effect of the resonator is very obvious.

The optical conductivity of the graphene sheet can be calculated using random-phase approximation in the local limit[21–23],

$$\begin{aligned}\sigma_s(\omega) = {} & \frac{i2e^2 k_B T}{\pi\hbar^2(\omega + i\tau^{-1})} \ln\left[2\cosh\left(\frac{E_F}{2k_B T}\right)\right] \\ & + \frac{e^2}{4\hbar}\left[\frac{1}{2} + \frac{1}{\pi}\arctan\left(\frac{\hbar\omega - 2E_F}{2k_B T}\right)\right. \\ & \left. - \frac{i}{2\pi}\ln\frac{(\hbar\omega + 2E_F)^2}{(\hbar\omega - 2E_F)^2 + 4(k_B T)^2}\right],\end{aligned} \tag{3}$$

where $e = 1.602 \times 10^{-19}$ C is the electronic charge, $k_B = 1.3806 \times 10^{-23}$ J/K is the Boltzmann constant, T is the temperature (300 K in this case), $\hbar = 1.0546 \times 10^{-34}$ J · S is the reduced Planck's constant, ω is the circular frequency of incident light, E_F is the Fermi level, and $\tau = \mu E_F/(ev_F^2)$ is the carrier relaxation lifetime[24], where $\mu = 10000$ cm^2 · V^{-1} · s^{-1} is the dc mobility[25] and $v_F \approx 1 \times 10^6$ m/s is the Fermi velocity.

Having obtained the conductivity of the graphene, it can be used to calculate its refractive index using the expression $n_G = \sqrt{\mu_r \varepsilon_r}$. Here, $\mu_r = 1$ is the relative permeability, and ε_r can be expressed as follows[21]:

$$\varepsilon_r = 1 + \frac{i\sigma_s(\omega)}{\omega\varepsilon_0 d}, \tag{4}$$

where $\varepsilon_0 = 8.8542 \times 10^{-12}$ F/m is the permittivity in a vacuum, and $d = 0.5$ nm is the thickness of the graphene

monolayer. In order to calculate the effective refractive index under the condition of having single-layer graphene, we first calculate the refractive index of graphene n_G among different Fermi levels as a function of the wavelengths. Then, we import the data to the Lumerica Mode solution and use the FVC method to calculate the effective refractive index of the waveguide n_c. In this Letter, we put only one layer of graphene in the sandwich structure because the single-layer graphene has little influence on the effective refractive index of a sandwich structure if the Fermi level of the graphene is tuned[26], and we just need a smaller adjustment range of the effective refractive index.

According to a previous description[27], only when the image part of the optical conductivity $\sigma_s(\omega) > 0$ can a graphene monolayer support the TM mode. Figure 3 shows that this requirement can be met when the Fermi level $0 < E_F < 0.08$ eV or 0.32 eV $< E_F < 1$ eV. Considering that a large adjustment range may be required, the Fermi level of $E_F > 0.32$ eV was chosen for our calculation. As demonstrated in Fig. 4(a), the real part of the refractive index of graphene $\mathrm{Re}(n_G)$ decreases with the wavelength among all Fermi levels, and importantly, the refractive index is approximately inversely proportional to the wavelength. Figure 4(b) is calculated from the FVC method, and the inverse relationship in it is due to the inverse relationship in Fig. 4(a). As shown in Fig. 4(c), through tuning the Fermi level of graphene in the range of 0.32 to 0.46 eV, we can let the resonator resonate in any position of the operation's wavelength range. As we mentioned above, the Fermi level of graphene must be bigger than 0.32 eV, so, in the resonance grade of $m = 29$, the resonance peaks can only be tuned from 2331.8 to 2297.4 nm (the position of the left dotted line). Fortunately, the rest of the resonance peaks can be obtained in the resonance grade $m = 28$. At the same time, the left and right red dotted lines are in the resonance grades of 30 and 29, respectively. The following analysis will be based on the two red dotted lines.

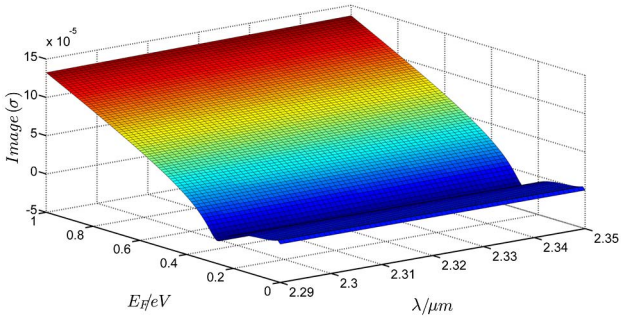

Fig. 3. Image part of the optical conductivity in the operation's wavelength range.

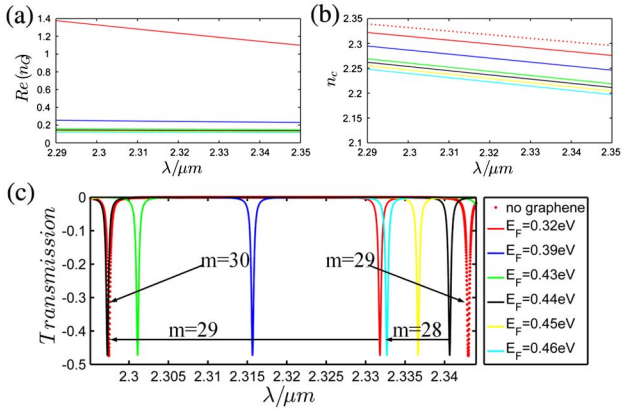

Fig. 4. (a) Real part of the refractive index of graphene $\mathrm{Re}(n_G)$ among different Fermi levels as a function of the incident light wavelength λ. (b) The effective refractive index with and without graphene. (c) The calculated transmission curve corresponding to the different effective refractive index curve in (b), and the red dotted line is the same as the dotted line in Fig. 2(a). The illustration of color line is suitable for all plots.

The Fermi level of graphene can be tuned by applying the voltage[16,28,29]

$$E_F = \hbar \nu_F (\pi a_0 |V_g - V_{\mathrm{Dirac}}|)^{1/2}, \tag{5}$$

where $a_0 = \varepsilon_{r1}\varepsilon_0/(d_1 e)$ is obtained from the simple capacitor model, $|V_g - V_{\mathrm{Dirac}}|$ is the applied voltage, and ε_{r1} and d_1 are the permittivity and thickness of the aluminum oxide layer (2.9791 and 10 nm, respectively). Figure 2 shows that the FWHM of the red dotted resonance peaks is about 1.5 nm, while the FSR is about 45 nm, so, in this experiment, we can get another 14 uniformly distributed characteristic peaks across the operation's wavelength range by controlling the applied voltage. The spectrum of our spectrometer is presented in Fig. 5. Note that the two resonance curves (black lines) on both sides of the spectrum are exactly the same as the red dotted line in Fig. 2, while the other 14 resonance curves (red lines) are obtained from tuning the applied voltage. The blue line in Fig. 5 shows the relationship between the resonant wavelength and applied voltage, whereas the 14 blue asterisks show the applied voltages that correspond to the 14 red resonance peaks. The dramatic change of voltage between 2.33 and 2.335 μm is because the resonance grade is changed from 29 to 28; in spite of this problem, by tuning the applied voltage within a small range (about 4 to 10 V),

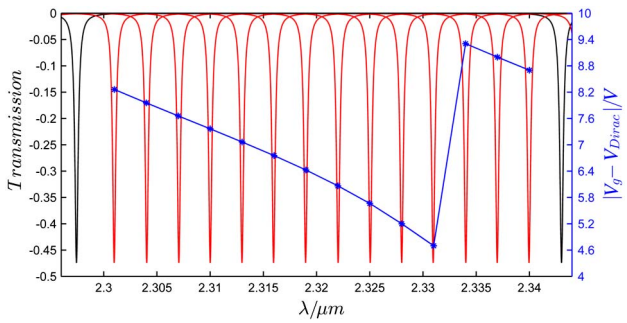

Fig. 5. Spectrometer spectrum (black and red line) and applied voltage (blue line) as a function of the incident light.

the resonant wavelength of the resonator can be dynamically tuned. Thus, we can obtain an integrated tunable spectrometer in the working wavelengths.

In conclusion, structure optimization makes it possible to obtain a micro-ring resonator with superior performance, with an FWHM of less than 1.5 nm and an FSR of about 45 nm. By combining this with a graphene monolayer, an on-chip tunable spectrometer with a working wavelength of 2.29 to 2.35 μm is proposed. By controlling the applied voltage, the resonant wavelength of the resonator can be dynamically tuned, thereby producing 16 characteristic peaks in the working wavelength range. This tunable spectrometer can have a significant effect on the development of on-chip spectrometers.

This work was supported by the Advanced Research Program of National University of Defense Technology (Nos. JC13-02-15 and JC13-02-13), the Natural Science Foundation of Hunan Province (Nos. 13JJ4008 and 13JJ3001), and the Program for New Century Excellent Talents in University (No. NCET-12-0142).

References

1. B. Momeni, S. Yegnanarayanan, M. Soltani, A. A. Eftekhar, E. S. Hosseini, and A. Adibi, J. Nanophoton. **3**, 031001 (2009).
2. H. I. Hsu, P. Wu, and C. Huang, Chin. Opt. Lett. **14**, 030501 (2016).
3. K. Kodate, Y. Komai, and K. Okamoto, J. Opt. A-Pure Appl. Op. **10**, 44011 (2008).
4. T. Fukazawa, F. Ohno, and T. Baba, Jpn. J. Appl. Phys. **43**, L673 (2004).
5. M. Muneeb, X. Chen, P. Verheyen, G. Lepage, S. Pathak, E. Ryckeboer, A. Malik, B. Kuyken, M. Nedeljkovic, J. V. Campenhout, G. Z. Mashanovich, and G. Roelkens, Opt. Express **21**, 11659 (2013).
6. A. Malik, M. Muneeb, S. Pathak, Y. Shimura, J. V. Campenhout, R. Loo, and G. Roelkens, IEEE Photon. Technol. Lett. **25**, 1805 (2013).
7. M. Muneeb, A. Vasiliev, A. Ruocco, A. Malik, H. Chen, M. Nedeljkovic, J. S. Penades, L. Cerutti, J. B. Rodriguez, G. Z. Mashanovich, M. K. Smit, E. Tourni, and G. Roelkens, Opt. Express **24**, 9465 (2016).
8. R. Wang, M. Muneeb, S. Sprengel, G. Boehm, A. Malik, R. Baets, M. Amann, and G. Roelkens, Opt. Express **24**, 8480 (2016).
9. A. Malik, M. Muneeb, Y. Shimura, J. V. Campenhout, R. Loo, and G. Roelkens, Appl. Phys. Lett. **103**, 161119 (2013).
10. Q. Zhou, J. Pang, X. Li, K. Ni, and R. Tian, Chin. Opt. Lett. **13**, 110501 (2015).
11. V. Velasco, P. Cheben, P. J. Bock, A. Delâge, J. H. Schmid, J. Lapointe, S. Janz, M. L. Calvo, D. Xu, M. Florjańczyk, and M. Vachon, Opt. Lett. **38**, 706 (2013).
12. M. Nedeljkovic, A. V. Velasco, A. Z. Khokhar, A. Delâge, P. Cheben, and G. Z. Mashanovich, IEEE Photon. Technol. Lett. **7**, 1 (2015).
13. Z. Xia, A. A. Eftekha, M. Soltani, B. Momeni, Q. Li, M. Chamanzar, S. Yegnanarayanan, and A. Adibi, Opt. Express **19**, 12356 (2011).
14. A. Malik, S. Dwivedi, L. V. Landschoot, M. Muneeb, Y. Shimura, G. Lepage, J. V. Campenhout, W. Vanherle, T. V. Opstal, R. Loo, and G. Roelkens, Opt. Express **22**, 28479 (2014).
15. M. R. Watts, W. A. Zortman, D. C. Trotter, G. N. Nielson, D. L. Luck, and R. W. Young, in *Conference on Lasers and Electro-Optics*, 1 (2009).
16. F. Wang, Y. Zhang, C. Tian, C. Girit, A. Zettl, M. Crommie, and Y. R. Shen, Science **320**, 206 (2008).
17. J. M. Dawlaty, S. Shivaraman, M. Chandrashekhar, F. Rana, and M. G. Spencer, Appl. Phys. Lett. **92**, 042116 (2008).
18. R. R. Nair, P. Blake, A. N. Grigorenko, K. S. Novoselov, T. J. Booth, T. Stauber, N. M. R. Peres, and A. K. Geim, Science **320**, 1308 (2008).
19. A. Yariv, Electron. Lett. **36**, 321 (2000).
20. C. Manolatou, M. J. Khan, S. Fan, P. R. Villeneuve, and H. A. Haus, IEEE J. Quantum Electron. **35**, 1322 (1999).
21. Y. Yao, M. A. Kats, P. Genevet, N. Yu, Y. Song, J. Kong, and F. Capasso, Nano Lett. **13**, 1257 (2013).
22. L. A. Falkovsky and S. S. Pershoguba, Phys. Rev. B **76**, 153410 (2007).
23. L. A. Falkovsky and A. A. Varlamov, Eur. Phys. J. B **56**, 281 (2007).
24. J. Zhang, Z. Zhu, W. Liu, X. Yuan, and S. Qin, Laser Sci. **1505**, 03016 (2015).
25. K. S. Novoselov, A. K. Geim, S. V. Morozov, D. Jiang, Y. Zhang, S. V. Dubonos, I. V. Grigorieva, and A. A. Firsov, Science **306**, 666 (2004).
26. S. Ye, Z. Wang, L. Tang, Y. Zhang, R. Lu, and Y. Liu, Opt. Express **22**, 26173 (2014).
27. A. Vakil and N. Engheta, Science **332**, 1291 (2011).
28. L. Ren, Q. Zhang, J. Yao, Z. Sun, R. Kaneko, Z. Yan, S. L. Nanot, Z. Jin, I. Kawayama, M. Tonouchi, J. M. Tour, and J. Kono, Nano Lett. **12**, 3711 (2012).
29. J. Yan, Y. Zhang, P. Kim, and A. Pinczuk, Phys. Rev. Lett. **98**, 166802 (2007).